Designing An Open-Source Power Inverter (Part 18): Transformer Winding Design For The Battery Converter—Secondary Winding Design

by Dennis Feucht, Innovatia Laboratories, Cayo, Belize

In the most recent installment in the Volksinverter design series,[1-17] part 17, the previously derived winding design procedure and formulas[16] were used to evaluate various winding configurations for the primary winding in the battery converter's transformer (Fig. 1). In this part, the same basic design procedure is now applied to the design of the secondary winding.

As determined in earlier parts in the series, the transformer has a single secondary winding with turns of

$$N_s = N_p \cdot (1/n) = 6 \cdot 4 = 24$$

As in the primary winding design, we have a winding configuration choice. For isolation and safety, a combination of primary and secondary windings in a multifilar unibundle require adequately insulated secondary (or primary) wire (such as Rubadue wire). However, use of such safety insulated wire reduces packing factor versus use of conventional magnet wire in combination with polyester insulating tape. So the thicker safety insulated wire is not considered here. A bobbin with plastic separator would be another option, though it is unlikely that a commercial bobbin with a 60/40% separation is available. (See part 16 for winding area allotment.)

We can either opt for two windings of $w_W/2$ width connected in parallel and wound over primary windings of the same width from Plans A through D (in part 17) or we can extend a single secondary winding across the full window width of w_W. In a parallel half-width option, winding spiral length is halved, and this can reduce both static and eddy-current winding resistance.[8] (PQ cores have a better shape than ETD cores for minimizing winding loss.)

All four windings are coupled through the common core. Each primary winding couples into both secondary windings in circuit operation, and pairing them does not have an advantage. The half-width option also requires more terminal pin connections. In view of this, a full-width (w_W) secondary winding is preferred in combination with primary winding plan F (or plan A).

The secondary winding area dimensions are

$$w_{WS} = 20.9 \text{ mm}; \; h_{WS} = (0.4) \cdot 6.0 \text{ mm} = 2.4 \text{ mm} \Rightarrow a_{WS} = 20.9 \text{ mm}/2.4 \text{ mm} = 8.71$$

Plans W through Y, which are described here, follow the scheme of electrically paralleling multiple layers to maximize window utilization. Plan Z changes the winding configuration to multifilar.

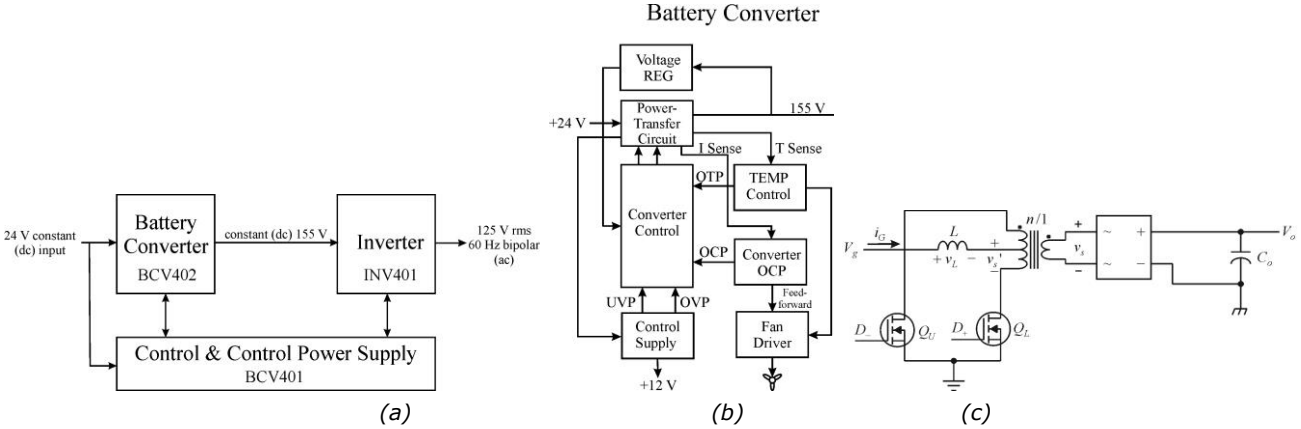

Fig. 1. The Volksinverter's system block diagram (a), the BCV402 battery converter stage block diagram (b) and the CA (boost) push-pull power-transfer circuit (BPP) (c). Here in part 18 discussion of the BPP transformer design continues with a focus on its secondary winding.

Plan W: Single-Strand Three-Layer Winding

Following the procedure of primary winding design, the closest integer fit of window aspect ratio is

$$a_{ws} \approx 8/1 = 24/3$$

Choose a secondary winding of M = 3 layers of N_{lb} = 24 turns per layer in parallel layers across winding window width w_w to a height of

$$h_w = 2\cdot(1 + \sqrt{3})\cdot r_{cw} \approx 5.464\cdot r_{cw} < h_{ws} = 2.4 \text{ mm}$$

Hexagonal packing offsets alternate layers to fit in the grooves of adjacent layers, thereby increasing packing though extending width by r_{cw}. If the turns per layer N_{lb} is large, $r_{cw} << w_w$. (Square packing has a height of $3\cdot(2\cdot r_{cw}) = 6\cdot r_{cw}$.) Solving for height fit,

$$r_{cw} = \frac{h_w}{2\cdot(1+\sqrt{3})} \approx (0.183)\cdot h_w = (0.183)\cdot(2.4 \text{ mm}) = 0.439 \text{ mm} \rightarrow r_{cw}(\#\,21) = 0.401 \text{ mm};\ I_{\max} = 1.88 \text{ A}$$

A horizontal fit gives wire radius

$$r_{cw} = \tfrac{1}{2}\cdot w_w / N_{lb} = (10.45 \text{ mm})/24 = 0.435 \text{ mm} > 0.401 \text{ mm}$$

Both dimensions allow for #21 wire. The utilized width and height are

$$24\cdot(2\cdot 0.401 \text{ mm}) = 19.25 \text{ mm} = (0.921)\cdot w_{ws}$$

$$(5.464)\cdot(0.401 \text{ mm}) = 2.19 \text{ mm} = (0.913)\cdot h_{ws}$$

The configuration of three parallel 24-turn layers utilizes 92% of the secondary winding window—an acceptable fit. Then three parallel #21 windings have ampacity $I_{\max}$ = 5.64 A;

$$\tilde{i}_s = (0.978)\cdot(5.64 \text{ A}) = \mathbf{5.52\ A}$$

At $V_{g\min}$ = 20 V and maximum primary current, $D = D'$ = 0.500. Then the secondary packing factor

$$\kappa_s = \tilde{i}_s / \bar{i}_s = 1/\sqrt{D'} \approx 1.414 \text{ at } V_g = 20 \text{ V}$$

$$\Rightarrow \bar{i}_s = \tilde{i}_s / \kappa_s \approx 5.52 \text{ A}/1.414 = 3.90 \text{ A}$$

The secondary winding (as three parallel windings) can transfer at constant secondary voltage V_s = 160 V,

$$\bar{P}_{s0} = V_s\cdot \bar{i}_s = (160 \text{ V})\cdot(3.90 \text{ A}) = \mathbf{624\ W}$$

This is the maximum static power without eddy-current effects at $V_{g\min}$. The winding resistance goal is

$$R_{wsopt} = \frac{\bar{P}_s}{\tilde{i}_s^2} = \frac{\psi_{\max}\cdot(\bar{P}_c/2)}{\tilde{i}_s^2} = \frac{0.952 \text{ W}}{\tilde{i}_s^2} = \frac{0.952 \text{ W}}{(5.52 \text{ A})^2} = 31.2 \text{ m}\Omega \Rightarrow$$

$$f_{ropt} = R_{wsopt}/R_{\delta r} = 31.2 \text{ m}\Omega/33 \text{ m}\Omega = 0.945$$

The Dowell plots in Fig. 3 of part 17—repeated below in Fig. 2—apply directly to the unbundled secondary winding of three electrically-parallel layers;

$$f_r = F_r(\#\,21, 3)/3 = 6.4/3 = 2.13 = (2.25)\cdot f_{ropt} = (2.25)\cdot(0.945)$$

At f = 75 kHz, #21 wire in Fig. 1 is at peak F_r, the worst-case wire size, maximizing eddy-current loss. Thus $\overline{P}_s$ will be constrained to well under $\overline{P}_{s0}$. Reverse calculation given $f_{ropt} = f_r$, results in $\tilde{i}_s$ = 2.60 A and $\overline{P}_{s0}$ = **294 W**. This is significantly less than the primary transfer power of 454 W.

Although the secondary window has more than adequate static power capability, its high eddy-current loss constrains it to about half the static power value. This design is close to a traditional single-strand, multilayer winding configuration and shows why eddy-current loss prevents it from achieving its static power value. Plan W is suboptimal and is rejected.

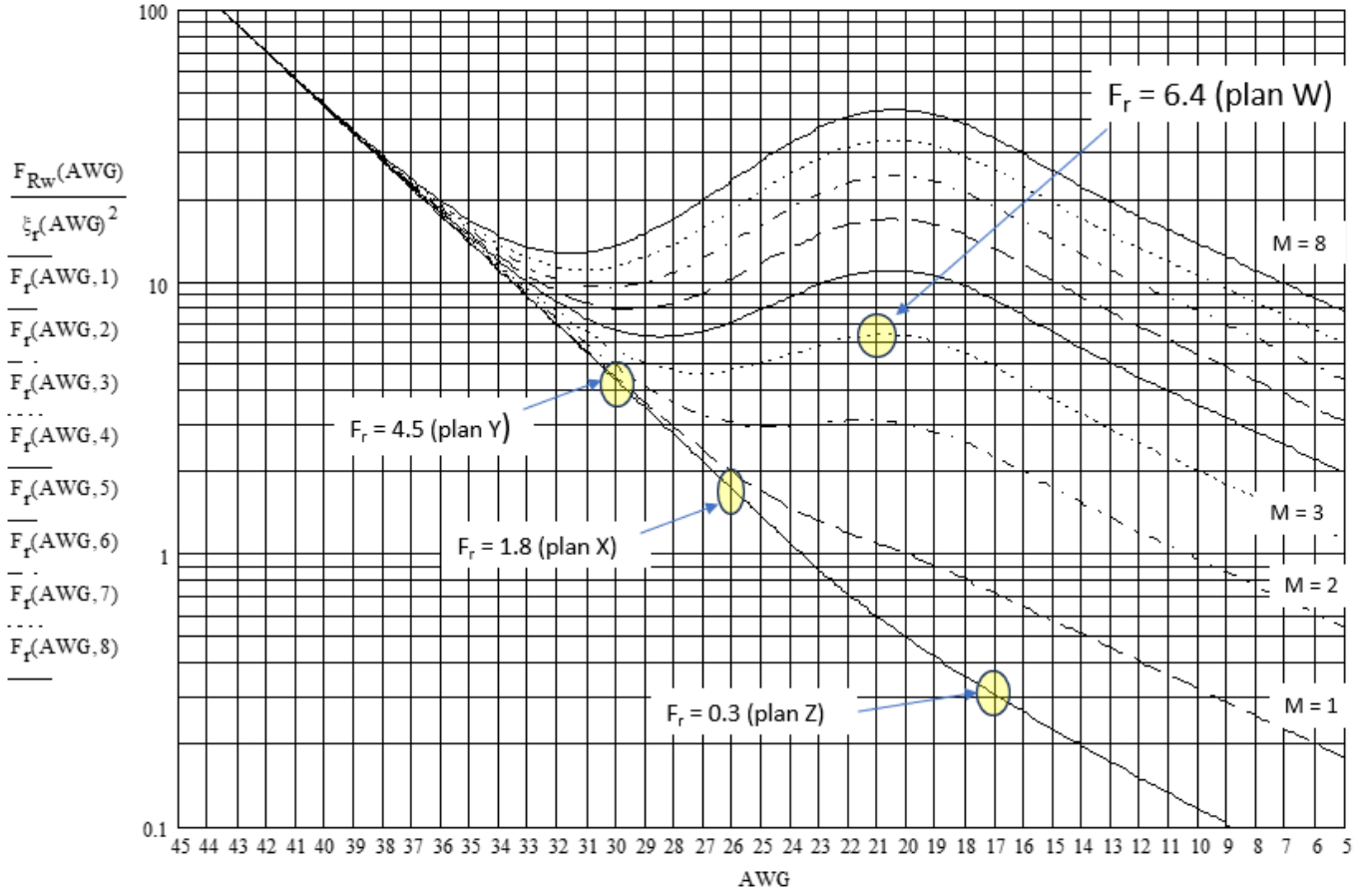

Fig. 2. Eddy-current resistance-ratio F_r at magnetic f = 75 kHz and $R_{\delta r}/l_w$ = 94.2 mΩ/m for Cu at 80°C. F_r(AWG, M) has winding layers M. The point of interest for plan W—F_r (AWG = #21, M = 3) = 6.4—is highlighted. F_r points of interest for other plans discussed in subsequent sections of this article are also identified.

Plan X: Twisted Three-Strand, Parallel Three-Layer Winding

A reduction in wire size from that of #21 wire decreases F_r from its worst-case value. The rationale for plan X is that strands of a twisted three-strand bundle will pack together better than two- or four-strand bundles and is reduced from plan W eddy-current effects. The allowable bundle radius for a horizontal fit of 24 turns is

$$r_{bw}' = \tfrac{1}{2}\cdot(20.9\text{ mm})/24 = 0.4354\text{ mm}$$

For bundle N_s = 3,[4]

$$r_{cw} = r_{bw}'/1.886 = 0.231\text{ mm} \Rightarrow r_{cw}(\#\,26) = 0.231\text{ mm} \Rightarrow$$

$$r_{bw}' = (0.231\text{ mm})\cdot(1.886) = 0.436\text{ mm}\ ;\ p = 30\cdot r_{bw}' = 13.1\text{ mm}$$

The M = 3 layers in square and hexagonal layering are

$$M_{sq} = (2.4\text{ mm})/2\cdot(0.436\text{ mm}) = 2.752 \Rightarrow M_{hex} = \frac{2\cdot(M_{sq}-1)}{\sqrt{3}} + 1 = 3.02 \approx 3$$

Hexagonal packing of three layers fills the window height, and secondary winding window utilization is excellent. Three parallel windings of #26 × 3 bundles have I_{max} = 9·(0.592 A) = 5.328 A. Adjusting for core size,

$$\tilde{\tilde{i}}_s = (0.978)\cdot(5.328\text{ A}) = \mathbf{5.21\ A}$$

The secondary winding current waveform is a square-wave of duty-ratio D'. For square-wave current,

$$\frac{\bar{i}_s}{\tilde{\tilde{i}}_s} = \frac{D'\cdot\hat{i}_s}{\sqrt{D'}\cdot\hat{i}_s} = \sqrt{D'} \Rightarrow \bar{i}_s = \sqrt{D'}\cdot\tilde{\tilde{i}}_s$$

Excerpted are the following circuit parameters for transformer design from Table 1 of part 15:

Table 1. Circuit parameters for battery-converter transformer design.

V_g (V)	20	25	30
D'	0.500	0.625	0.750
$\tilde{\tilde{i}}_s$ (A)	4.42	3.95	3.61

The average secondary current over the V_g range is independent of V_g;

$$\bar{i}_s = \tilde{\tilde{i}}_s\cdot\sqrt{D'} = 3.125\text{ A}$$

Static power is thus

$$\bar{P}_{s0} = V_{g\min}\cdot\bar{i}_s(\max) = (160\text{ V})\cdot(3.125\text{ A}) = \mathbf{500\ W}$$

For optimal winding-to-winding power transfer, optimal secondary resistance is

$$R_{wsopt} \approx \frac{0.952\text{ W}}{(5.21\text{ A})^2} = 35.1\text{ m}\Omega$$

From the "Bundle Length" section of part 17 (the primary winding design),

$$\bar{r}_s = r_o - \frac{(0.4)\cdot h_w}{2} = 11.5\text{ mm};\ l_{ws}' = l_{ws}/k_{tw} = (2\cdot\pi\cdot\bar{r}_s\cdot N_s + M_s\cdot w_w)/k_{tw} = 176.95\text{ cm} + (2.133\text{ cm})\cdot M_s$$

For each of three secondary windings in parallel, M_s = 1 and

$$l_{ws}/k_{tw} = [2\cdot\pi\cdot\bar{r}_s\cdot N_p/n + M_s\cdot w_w]/k_{tw} = [176.95\text{ cm} + (1)\cdot(2.133\text{ cm})]/(0.9788) = 179.1\text{ cm} \rightarrow 185\text{ cm}$$

(Layer length varies from this average based on average winding radius from the core center and should be refined for the first and third layers. The small length differences between layers will also cause some small current imbalance among layers.)

Secondary $R_{\delta r} = (0.125\,\Omega/\text{m}) \cdot l_{ws}$ = 23.125 mΩ. Then the eddy-current goal for f_r is

$$f_{ropt} = R_{wsopt}/R_{\delta r} = 35.1\ \text{m}\Omega/23.125\ \text{m}\Omega = 1.52$$

Twisted strands for N_s < 5, have only strand skin-effects. The nine strands in total have

$$f_r = f_{rw}(\#\,26) = F_{rw}(\#\,26)/3{\cdot}3 = 1.8/9 = 0.20 < f_{ropt} = 1.52$$

The three-strand twisted bundle of plan X appreciably reduces winding loss over the single-strand plan W. Three layers of twisted three-strand bundles produce an interbundle field but nullify the interbundle proximity-effect. The bundle skin-effect is minimal for less than five (stacked) bundles, leaving the above f_r value.

With $f_r << f_{ropt}$, secondary winding loss is much lower than at maximum power transfer across windings (at $f_r = f_{ropt}$) and power-transfer efficiency variation at the low-current end of the operating range is also greater.

To recap, plan X is

Three parallel layers of 24 turns each of twisted #26 × 3 across full width w_w of winding window; p = 13 mm

Plan Y: Five-Strand, Parallel Three-Layer Winding

Retaining the parallel-layer winding configuration, a final strand iteration of three paralleled windings, one per 24-turn layer, takes N_s to the limit of what can nullify most eddy-current effects, at N_s = 5. The procedure follows that of plans W and X with minimal comment:

$$r_{bw}' = ½{\cdot}(20.9\ \text{mm})/24 = 0.4354\ \text{mm};\ N_s = 5 \Rightarrow r_{cw} = r_{bw}'/2.646 = 0.165\ \text{mm} \Rightarrow \#\,30 \Rightarrow r_{cw} = 0.150\ \text{mm} \Rightarrow$$

$$r_{bw}' = (0.15\ \text{mm}){\cdot}(2.646) = 0.397\ \text{mm} \Rightarrow p = 30{\cdot}(0.397\ \text{mm}) = 11.9\ \text{mm}$$

$$M = (2.4\ \text{mm})/2{\cdot}(0.397\ \text{mm}) = 3.023\ \approx 3$$

Size #29 wire almost fits (r_{cw}(#29) = 0.167 mm), although bundle compression is avoided and area margin increased with the smaller wire size. The winding consists of three electrically-parallel layers of #30 × 5 windings. They have ampacity

$$I_{\max} = 15{\cdot}(0.235\ \text{A}) = 3.525\ \text{A};\ \tilde{i}_s = (0.978){\cdot}(3.525\ \text{A}) = \mathbf{3.45\ A} \Rightarrow \bar{i}_s = 3.45\ \text{A}/1.414 = 2.44\ \text{A} \Rightarrow$$

$$\overline{P}_{s0} = V_s{\cdot}\bar{i}_s = (160\ \text{V}){\cdot}(2.44\ \text{A}) = \mathbf{390\ W}$$

Each of the three parallel layers has length

$$l_{ws}/k_{tw} = [2\cdot\pi\cdot\bar{r}_s\cdot N_p/n + M_s\cdot w_w]/k_{tw} = [180.6\ \text{cm} + (1){\cdot}(2.133\ \text{cm})]/(0.9788) = 186.7\ \text{cm} \rightarrow 192\ \text{cm}$$

$$R_{\delta r} = (0.125\,\Omega/\text{m})\cdot l_{ws} = 24\ \text{m}\Omega \Rightarrow R_{wsopt} \approx \frac{0.952\ \text{W}}{(3.45\ \text{A})^2} = 80.0\ \text{m}\Omega \Rightarrow f_{ropt} = 80.0\ \text{m}\Omega/24\ \text{m}\Omega = 3.33$$

Twisted strands for N_s < 5 have only strand skin-effects;

$$f_r = f_{rw}(\#\,30) = F_{rw}(\#\,30)/15 = 4.5/15 = 0.30 < 3.33$$

The bundle resistance ratio f_r is much less than f_{ropt} and is the best plan yet for minimizing eddy-current resistance loss. However, the efficiency curve is more peaked and closer to the low-current end of the operating range. Conductor packing is less and transfers less static power than plan X.

Once again, to summarize, plan Y is

Three electrically parallel layers of 24 turns of twisted #30 × 5 across winding window, w_w; p = 12 mm

Plan Z: Eight-Turn Bundle Of Three Strands

This plan deviates from plans W through Y by filling the secondary area of aspect ratio a_{ws} = 8.71 with an 8 × 1 multifilar bundle of eight turns of h_{ws} height that fills most of the w_w width. A single twisted bundle of three strands is easiest to wind. Instead of geometrically-parallel layers, the turns are twisted together in a single bundle and then connected electrically in series.

The strand ends are separated and attached to bobbin pins connected in series to result in 24 turns. (The dotted end of the first strand of eight turns connects to the undotted end of the next strand whose dotted end connects to the undotted end of the final strand. The winding is across the dotted end of this third strand to the undotted end of the first strand.) The bundle is larger than those of the three-layer plans, giving each strand greater ampacity, though the winding current density remains to be calculated.

Working through the calculations for plan Z, three strands are chosen for the most compact bundle with radius

$$r_{bw}' = ½\cdot(2.4\text{ mm}) = 1.2\text{ mm}$$

Following the wire-size calculations of the previous plans, for bundle N_s = 3,[4]

$$r_{cw} = r_{bw}'/1.886 = 0.636\text{ mm} \Rightarrow r_{cw}(\#\,17) = 0.625\text{ mm} \Rightarrow$$

$$r_{bw}' = (0.225\text{ mm})\cdot(1.886) = 0.424\text{ mm};\ p = 30\cdot r_{bw}' = 12.7\text{ mm}$$

$$I_{\max}(\#\,17) = 4.738\text{ A} \Rightarrow \tilde{i}_s = (0.978)\cdot(4.738\text{ A}) = \mathbf{4.63\ A}$$

Average secondary current, calculated at $V_{g\min}$ = 20 V, and static power are

$$\bar{i}_s \approx \tilde{i}_s\cdot\sqrt{D'} = (4.63\text{ A})\cdot(0.7071) = 3.28\text{ A}$$

$$\bar{P}_{s0} = V_{g\min}\cdot\bar{i}_s = (160\text{ V})\cdot(3.28\text{ A}) = \mathbf{524\ W}$$

For optimal winding-to-winding power transfer,

$$R_{wsopt} \approx \frac{0.952\text{ W}}{(4.63\text{ A})^2} = 44.4\text{ m}\Omega$$

From the bundle length formula in plan X,

$$\bar{r}_s = r_o - \frac{(0.4)\cdot h_w}{2} = 11.5\text{ mm};\ l_{ws}' = l_{ws}/k_{tw} = (2\cdot\pi\cdot\bar{r}_s\cdot N_s + M_s\cdot w_w)/k_{tw} = 176.95\text{ cm} + (2.133\text{ cm})\cdot M_s$$

For each of three strands electrically in series, secondary layers M_s = 1, and

$$l_{ws}' = l_{ws}/k_{tw} = [2\cdot\pi\cdot\bar{r}_s\cdot N_p/n + M_s\cdot w_w]/k_{tw}$$

$$= [176.95\text{ cm} + (1)\cdot(2.133\text{ cm})]/(0.9788) = 179.1\text{ cm} \rightarrow 185\text{ cm}$$

This length is that of the twisted bundle and applies to all three strands because they share the average r_s of the bundle. Secondary $R_{\delta r} = (0.125\,\Omega/\text{m}) \cdot l_{ws}$ = 23.125 mΩ. Then the eddy-current goal for f_r is

$$f_{ropt} = R_{wsopt}/R_{\delta r} = 44.4\ \text{m}\Omega/23.125\ \text{m}\Omega = 1.92$$

Twisted strands for N_s = 3 < 5 have only strand skin-effects. Then with strands in series, secondary winding

$$f_r = 3{\cdot}f_{rw}(\#\,17) = 3{\cdot}F_{rw}(\#17) = 3{\cdot}(0.30) = 0.90 < f_{ropt} = 1.92$$

The bundle f_r winding resistance is lower than that of f_{ropt} but close enough for broad transfer efficiency over the current range.

Once again, for reference, plan Z is

Three series strands of eight turns each of a twisted #17 × 3 bundle across width w_W of winding window; p = 13 mm

Summary Of Winding Plans

The calculated plans for the ETD34 secondary winding are summarized in Table 2. Instead of going through the reverse procedure to find $\overline{P}_s(f_{ropt})$, it is calculated from

$$\overline{P}_s(f_{ropt}) = \min\left\{\sqrt{\frac{f_{ropt}}{f_r}}\cdot\overline{P}_{s0}, \overline{P}_{s0}\right\}$$

Whenever $f_r > f_{ropt}$, excessive winding resistance causes $\overline{P}_s(f_{ropt}) < \overline{P}_{s0}$. $\overline{P}_s(f_{ropt})$ is not allowed to exceed static transfer power $\overline{P}_{s0}$ because it is derived from wire ampacity rating $I_{\max}$, the maximum static current based on the winding thermal model for wire. $I_{\max}$ determines $\tilde{i}_p$ from which R_{wsopt} and f_{ropt} are derived. The range of F_r, F_{rw}, f_r and f_{rw} is [0+, ∞). If f_r results in a lower R_{wsopt} and a higher $\tilde{i}_p$, then $\tilde{i}_p$ is limited by wire ampacity and not by the winding resistance at maximum power transfer, derived from the core thermal model.

Table 2. Alternative plans for ETD34 secondary windings.

Plan	N_s	Bundling	r_{cw}, AWG	$\tilde{i}_p$, A	$\overline{P}_{s0}$, W	$\overline{P}_s(f_{ropt})$, W	f_{ropt}	f_r	f_r/f_{ropt}
W	1	3||layers	21	5.52	624	294	0.945	2.13	2.25
X	3	3||bundles	26	5.21	500	500	1.52	0.20	0.132
Y	5	2||bundles	30	3.45	390	390	3.33	0.30	0.090
Z	3×2	bifilar	17	4.63	524	524	1.92	0.90	0.469

Primary-winding plan F and secondary plan Z are chosen for the Volksinverter design. Both use #17 wire which simplifies construction. Secondary plans X through Z have lower winding resistance than R_{wpopt}, and having lower winding loss, they trade off core and winding losses for a shift in maximum power transfer efficiency $\eta_{\max}$ to less than full-scale current. The eddy-current rules for twisted bundles greatly simplifies winding design, and though they are simplistic compared to FEA simulation for accuracy, they make design by calculator (or Mathcad) feasible while accounting for these complicating effects.

References

Except for the last reference, which comes from the APEC 2003 proceedings, all of the following works were published in the How2Power Today newsletter in the issues indicated. However, many of the same concepts are covered in the author's power-electronics books, which are available for download at innovatia.com.

1. "Designing An Open-Source Power Inverter (Part 1): Goals And Specifications" by Dennis Feucht, How2Power Today, May 2021.
2. "Designing An Open-Source Power Inverter (Part 2): Waveshape Selection" by Dennis Feucht, How2Power Today, September 2021.
3. "Designing An Open-Source Power Inverter (Part 3): Power-Transfer Circuit Options" by Dennis Feucht, How2Power Today, April 2022.
4. "Designing An Open-Source Power Inverter (Part 4): The Optimal Power-Line Waveshape" by Dennis Feucht, How2Power Today, May 2022.
5. "Designing An Open-Source Power Inverter (Part 5): Kilowatt Inverter Circuit Design" by Dennis Feucht, How2Power Today, July 2022.
6. "Designing An Open-Source Power Inverter (Part 6): Kilowatt Inverter Control Circuits" by Dennis Feucht, How2Power Today, August 2022.
7. "Designing An Open-Source Power Inverter (Part 7): Kilowatt Inverter Magnetics" by Dennis Feucht, How2Power Today, September 2022.
8. "Designing An Open-Source Power Inverter (Part 8): Converter Control Power Supply" by Dennis Feucht, How2Power Today, November 2022.
9. "Designing An Open-Source Power Inverter (Part 9): Magnetics For The Converter Control Power Supply" by Dennis Feucht, How2Power Today, December 2022.
10. "Designing An Open-Source Power Inverter (Part 10): Converter Protection Circuits" by Dennis Feucht, How2Power Today, February 2023.
11. "Designing An Open-Source Power Inverter (Part 11): Minimizing Switch Loss In Low-Input-Resistance Converters" by Dennis Feucht, How2Power Today, March 2023.
12. "Designing An Open-Source Power Inverter (Part 12): Sizing The Converter Magnetics" by Dennis Feucht, How2Power Today, May 2023.
13. "Designing An Open-Source Power Inverter (Part 13): The Differential Boost Push-Pull Power-Transfer Circuit" by Dennis Feucht, How2Power Today, June 2023.
14. "Designing An Open-Source Power Inverter (Part 14): Boost Push-Pull Or Buck Bridge?" by Dennis Feucht, How2Power Today, July 2023
15. "Designing An Open-Source Power Inverter (Part 15): Transformer Magnetic Design For the Battery Converter" by Dennis Feucht, How2Power Today, March 2024.
16. "Designing An Open-Source Power Inverter (Part 16): Transformer Winding Design For the Battery Converter—Efficiency Range And Winding Allotment" by Dennis Feucht, How2Power Today, April 2024.
17. "Designing An Open-Source Power Inverter (Part 17): Transformer Winding Design For the Battery Converter—Alternative Configurations" by Dennis Feucht, How2Power Today, May 2024.
18. "The Geometry of Twisted Wire Bundles" by Dennis Feucht, How2Power Today, July 2018.
19. "How Twisted Bundles Reduce Eddy-Current Effects In Winding Bundle Design" by Dennis Feucht, How2Power Today, September 2023.
20. "Magnetizing Current and Transformer Design Optimization" by Dennis Feucht, How2Power Today, October 2023.
21. "How Wire Bundle Configurations Influence Eddy-Current Proximity Effects" by Dennis Feucht, How2Power Today, February 2019.
22. "Bundle Compression Overcomes Aspect Ratio Constraints On Transformer Design," by Dennis Feucht, How2Power Today, June 2018.
23. "Optimal Core Dimensional Ratios for Minimizing Winding Loss in High-Frequency Gapped-Inductor Windings" by R. Jensen and C. R. Sullivan, *IEEE Applied Power Electronics Conference*, FEB03, pp. 1164-1169.

About The Author

Dennis Feucht has been involved in power electronics for 40 years, designing motor-drives and power converters. He has an instrument background from Tektronix, where he designed test and measurement equipment and did research in Tek Labs. He has lately been working on projects in theoretical magnetics and power converter research.

For more on magnetics design, see these How2Power Design Guide search results.